ADVANCED SUSTAINABLE SYSTEMS
www.advsustainsys.com

Novel Graphene-Based Foam Composite As a Highly Reactive Filter Medium for the Efficient Removal of Gemfibrozil from (Waste)Water

Ahmed M. E. Khalil, Lei Han, Ibrahim Maamoun, Tanveer A. Tabish, Yu Chen, Osama Eljamal, Shaowei Zhang, David Butler, and Fayyaz A. Memon**

Graphene-based materials have emerged as alternative adsorbents, but their success in removing pharmaceutical contaminants has been limited due to degradation caused by restacking and limited control over their sizes and porosities. Driven by this issue, in the current study, to counteract the restacking behavior, graphene sheets are supported on a thread/rod-like matrix structure in a boron nitride foam material, and a novel porous composite foam-supported graphene is synthesized. The as-prepared novel composite offers extraordinary features, such as high absorption kinetics, large available surface area, high porosity (>98%), ecofriendliness and cost-effective synthesis, and excellent affinity to emerging pharmaceutical contaminants. When batch-testing graphene-based foam material and porous graphene nanosheets to remove gemfibrozil (GEM) from wastewater samples, rapid adsorption kinetics (<5 min) are exhibited by the graphene-based foam. Column filter studies are conducted for both materials to test their performance in removing GEM from distilled water, synthetic graywater, and actual wastewater. Overall, the foam composite-based filter marginally outperforms the sand-supported graphene filter and significantly outperforms the unsupported graphene filter. A numerical MATLAB model is developed to simulate the reactive solute transport of GEM influent through the foam filter. Also, a formal sensitivity analysis is conducted to identify the key parameters influencing the model results.

1. Introduction

Pharmaceuticals are one class of the most noticeable emerging contaminants (ECs) in water bodies because of their unrecognized acute and chronic toxic characteristics. They can cause major ecological concerns as well as possible health risks.[1] For example, gemfibrozil (GEM) is used as a pharmaceutical to regulate blood lipids and treat high triglyceride and cholesterol levels in patients with pancreatitis.[1b] However, it is unclear whether its presence in water poses any environmental threat to humans and marine life, although some research reports have shown that it can lower testosterone levels in goldfish.[2] Also, GEM has a high biodegradation resistance, and, therefore, can be found in effluents from wastewater treatment plants/facilities (WWTPs) in some European countries at concentrations as high as 4.76 g L^{-1}.[3] Overall, the existing conventional technologies are incapable of removing this pharmaceutical impurity.[4] Therefore, it is critical for

A. M. E. Khalil, L. Han, Y. Chen, S. Zhang, D. Butler, F. A. Memon
College of Engineering
Mathematics and Physical Sciences
University of Exeter
Exeter, Devon EX4 4QF, UK
E-mail: a.a.khalil@exeter.ac.uk; F.A.Memon@exeter.ac.uk

A. M. E. Khalil
Department of Chemical Engineering
Faculty of Engineering
Cairo University
Giza 12613, Egypt

The ORCID identification number(s) for the author(s) of this article can be found under https://doi.org/10.1002/adsu.202200016.

L. Han
The State Key Laboratory of Refractories and Metallurgy
Wuhan University of Science and Technology
Wuhan 430081, China

I. Maamoun, O. Eljamal
Department of Earth System Science and Technology
Interdisciplinary Graduate School of Engineering Sciences
Kyushu University
6-1 Kasuga-Koen, Kasuga, Fukuoka 816-8580, Japan

I. Maamoun
Advanced Science Research Center
Japan Atomic Energy Agency
Tokai, Ibaraki 319-1195, Japan

T. A. Tabish
Wellcome Centre for Human Genetics
University of Oxford
Oxford OX3 7BN, UK

DOI: 10.1002/adsu.202200016

wastewater/drinking water treatment works to use efficient tertiary treatment technologies to effectively eliminate ECs from their treated effluent streams.

Adsorption is considered to be a promising technique, a reliable water treatment strategy, and a more cost-effective method than other important techniques, such as oxidation, reverse osmosis, ion exchange, microfiltration, and ultrafiltration, and so forth.[4a,5] The most distinct advantages of applying adsorption to water remediation include, e.g., ease of operation, abundance of numerous types of adsorbents, low cost, as well as the capability of removing most kinds of pollutants (e.g., organic/inorganic, soluble/insoluble, or biological.[6] However, the adsorption method for water treatment suffers from some limitations in its commercial use, in particular, the lack of high capacity adsorbents for a wide range of ECs.[4] Fortunately, graphene-based materials stood out from several other candidate adsorbents attempted, exhibiting promising performance in this aspect.[4b,7]

Owing to its high "intrinsic" specific surface area (i.e., compared to other carbon-based materials), hydrophobicity, monolayered structure, and the oxygen-containing functional groups (OCFGs) decorated surface, graphene and graphene oxide (GO) show a strong adsorption affinity for organic pollutants.[8] In our previous work, despite the efficient adsorption performance and reliable recyclability of porous graphene (PG) toward numerous ECs, the difficulty in separating such graphene-based materials (GBMs) from water, as well as their limited recyclability, restricts their practical applications in large-scale water purification.[9] Besides, another major issue hindering their application is aggregation/restacking among their sheets. This aggregation can return the GBM to its original raw material (graphite) via restacking.[10] Therefore, GBMs supported on a 3-D foam substrate could make the active sites on the two basal planes of segregated graphene sheets available for contaminant removal, since the support could disband the graphene nanosheet agglomeration and avoid or alleviate the restacking of graphene sheets during the water treatment process. In addition, the 3-D porous foam support filter medium itself possesses several outstanding physical properties, such as high porosity and specific surface area, low pressure drop, good adsorption performance, and better recyclability than its powdered adsorption counterparts, and hence is considered to be well suited to water treatment applications.[10b,11]

Despite the important roles played by 3D porous graphene materials in wastewater treatment, there are still some urgent issues that need to be addressed appropriately, including the significantly low mechanical strength, high cost, and multistep complex preparation processes, which limit their large-scale applications in harsh and real-world environments.[12] Given these, a new cost-effective, facile, and efficient synthesis approach is needed to develop the desired GBM foams for the removal of ECs.

Compared with the abovementioned 3D adsorbents, ceramic foams also have some advantages, such as low cost, good mechanical property, good stability, and environmental friendliness.[12c,13] Nonetheless, their adsorption ability is generally low, and most of them have no selective adsorption capacity. Therefore, functionalization via surface modification is considered to be an effective way to prepare foams for wastewater treatment.[12c,14] Several techniques have recently been used to modify diatomite foams to enhance their adsorption efficiency.[12c,13] However, the processes were relatively complex, and released lots of greenhouse gases. Fortunately, boron nitride (BN) has a variety of excellent properties such as good thermal stability, abrasion resistance, and strong chemical stability; therefore, it is used in high-temperature environment and by other sectors.[15] According to Xue et al., the prepared BN foams showed good performance in the adsorption of oils, Cd^{2+}, and rhodamine B.[15c] In terms of application, up to date, there have been few studies on the use of graphene or boron nitride materials for the treatment of pharmaceutical contamination (e.g., ciprofloxacin or CIP, GEM, and others), and even fewer studies on their recyclability.[4b,16] Hence, one of the main novelty features of this work is filling the knowledge gap in the literature on such aspects, which shall be a vital step toward the pilot-scale water treatment applications of foam-supported graphene materials. This cost-effective, low-head-loss novel graphene-based foam composite filter application will contribute to progress towards achieving the United Nation's Sustainable Development Goal of clean water and sanitation.

The present work aims to test the feasibility and efficacy of a novel supported (reduced) graphene oxide-BN foam (GO/BNF), synthesized via a simple foam-gel casting route, as a highly reactive filter medium for decontaminating gemfibrozil from normal water and wastewater. The as-prepared GO/BNF was used for the adsorption/removal of GEM pharmaceutical from aqueous media. Furthermore, the adsorption properties of as-prepared foams were studied using different adsorption equilibrium models, and the results were discussed to elucidate the adsorption behavior. In addition, mechanisms and spontaneity of adsorption were further illustrated by calculating the equilibrium parameters. The reusability of GO/BNF was investigated in several cycles. For future applications, column studies were conducted in which an adsorption column filter packed with GO/BNF was used for continuous assessment of the performance of GO/BNF in the GEM removal from normal water, simulated graywater and actual wastewater, evaluating the viability of the GO/BNF filter as a tertiary treatment option for wastewater treatment. Finally, a numerical model was applied to simulate the 1-D advective-dispersive reactive transport of GEM through the GO/BNF-based filter media in the columns investigated.

2. Experimental Section

2.1. Chemicals, Adsorbates and Adsorbents Preparation

Nano graphene platelets (NGP, ≈25 μm, surface area ≈100 m^2 g^{-1}), melamine (99%), boric acid (≥99.5%), hexadecyltrimethylammonium bromide (CTAB, ≥ 99%) and analytical grade pharmaceutical GEM, were purchased from Sigma-Aldrich Co. (Poole, Dorset, UK). Graphene oxide was prepared following the well-documented modified Hummers' method, as reported in our previous papers.[4b,7c]

Graphene oxide-BN foams (GO/BNF) and BN foams (BNF) were prepared using a foam-gelcasting method similar to that reported previously by us.[12c,13] The batch compositions for their

preparations are listed in Table S1 (Supporting Information). Typically, melamine (3.5 g), H_3BO_3 (3.5 g), and GO (50 mg) were dispersed in water (150 mL) under magnetic stirring at 353 K for 10 min to form a uniform solution. A foam slurry was prepared by adding CTAB (112.5 mg) into the solution under continuous magnetic stirring for about 2 min, and subsequent natural cooling to about 323 K under continuous stirring. The resultant slurry was immediately cast into a mold, and gelled at 298 K for 12 h. The obtained samples were dried at 353 K for 12 h before being heated at 3 K min^{-1} to 1423 K and held for 3 h in flowing N_2 atmosphere. Except for the absence of GO, the preparation process of BNF was essentially the same as that used for GO/BNF.

The pharmaceutical GEM and distilled water (DW) were used to prepare standard stock solutions of contaminant (at a high concentration of 10.5 mg L^{-1} and a low concentration of 1 mg L^{-1}) which were covered by aluminum foil during storage and tests to avoid photo-degradation of the contaminant.

Water samples were prepared from different types of water (distilled water, simulated graywater, and wastewater). The pharmaceutical solutions prepared above were used in batch tests to investigate the adsorption capacity and kinetics of the foams. Regarding the column tests, GEM-contaminated DW at 10.5 mg L^{-1} was introduced to the column filters to be investigated as a single contaminant solution. Additionally, six pharmaceutical contaminants (including GEM) were mixed together in three solutions of three different water bodies. A mixture of contaminants solution was tested as ideal (DW) and synthesized/simulated (grey and waste) water samples, which were used to simulate real sample investigations. Five widely consumed pharmaceuticals (atenolol (ATL), carbamazepine (CBZ), ciprofloxacin (CIP), diclofenac (DCF), and ibuprofen (IBP), purchased from Sigma-Aldrich Co.) were spiked into the GEM solution, which would interfere with the adsorption behavior of GO/BNF (foam material) towards GEM. The content of each pharmaceutical in DW (distilled Water), SGW (simulated graywater) and MWW (municipal wastewater) solutions was set to 1 mg L^{-1}. Synthetic graywater (SGW) was produced using the composition given in Table S2 (Supporting Information),[17] and its water quality characteristics are listed in Table S3 (Supporting Information). The materials tabulated in Table S2 (Supporting Information) were purchased as analytical grade chemicals and brought from Sigma-Aldrich Co. (Poole, Dorset, UK). They were used to synthesize SGW, which was spiked with six drugs, including GEM. In another water sample, the MWW was modified to contain the six drug contaminations at 1 mg L^{-1} each (6 mg L^{-1} as total) to be reduced by the foam material to trace concentrations as desired for water remediation. The partially treated MWW sample was taken from the final sedimentation tank of a secondary treatment unit located in a wastewater treatment work based in Devon, UK, and the properties of that effluent are shown in Table S4 (Supporting Information). After collection, the MWW sample was stored below 5 °C in a refrigerated store and was ready to be processed as an influent for the packed column filter tests within one week. All abovementioned pharmaceuticals-contaminated water samples (DW, SGW and MWW) were charged/pumped into the packed adsorption column filters for filtration studies and for monitoring the performance of the foam material in the column tests.

2.2. Batch Tests

The adsorption kinetics of adsorbent materials for GEM contaminants at an initial concentration (C_0) of 10.5 mg L^{-1} (stock solution) was examined at room temperature without adjusting the pH value. Pharmaceutical solutions (20 mL) were placed in bottles with screw caps (60 mL). Adsorbents (GO, NGP, BNF, and GO/BNF, 5 mg each) were added into the pharmaceutical solution, followed by magnetic stirring/mixing for predetermined periods (time t = 10, 20, 30, 40, 50, or 60 min). Samples were collected with syringes and filtered immediately using a 0.2 µm membrane filter.

Moreover, equilibrium adsorption tests were also carried out to evaluate the maximum equilibrium adsorption capacity of the adsorbents. A mixture of pharmaceutical solution (20 mL) and a certain amount of BNF or GO/BNF (0.1, 0.3, 0.5. 0.7, 1, 3 or 5 mg) were shaken in centrifuge tubes (50 mL) on a rotary shaker for 24 h. The supernatants were acquired after vacuum filtration. Tests were replicated three times and average values were reported and compared.

2.3. Column Tests

Column adsorption tests were conducted to specifically assess the applicability of GO/BNF as a filter packing for tertiary treatment of water and wastewater. Acrylic glass columns were utilized as filters with two different dimensional sizes; one with 100 mm in height and an inside diameter (ID) of 40 mm, and another with the same height (100 mm) but with a different ID of 18 mm. Sand, graphene, or foam particles were kept inside the filter by a wrapped sheet of stainless-steel mesh. The pharmaceutical solution of GEM in distilled water, simulated graywater or actual wastewater was introduced to the column filter from the bottom to the top (up-flow mode) via a peristaltic pump (323S/D, Watson Marlow, Cornwall, UK). The filtered discharge was collected in a receiving container. The filter system was illustrated in **Figure 1**. All the tests were triplicated/duplicated, and the average results were presented.

2.3.1. Column Study on GEM Single Solution

Column tests were conducted to assess the efficacy of porous graphene (PG) and GO/BNF materials as filter media to remove GEM (10.5 mg L^{-1}) from its distilled water solution. The filter bed was made from pure silica sand of 50–70 mesh, procured from Sigma Aldrich Co. In the column filter with 40 mm in ID, a single layer of dry GO/BNF adsorbent (3 mm thick) was introduced, on top of which a 50 mm thick sand layer was put, then another uniformly distributed adsorbent layer, and then another 50 mm thick sand layer. In the column tests for PG adsorbent, an adsorbent slurry/suspension was made via mixing a given quantity of 100 mg PG with 25 mL of deionized water, which was then subjected to 20 min ultrasonication to disperse the adsorbent. Sand was then added to the column in layers and "wet packed" with deionized water. A layer of slurry was then uniformly dispersed across the sand layer by a pipette. This process continued until the column was fully packed with

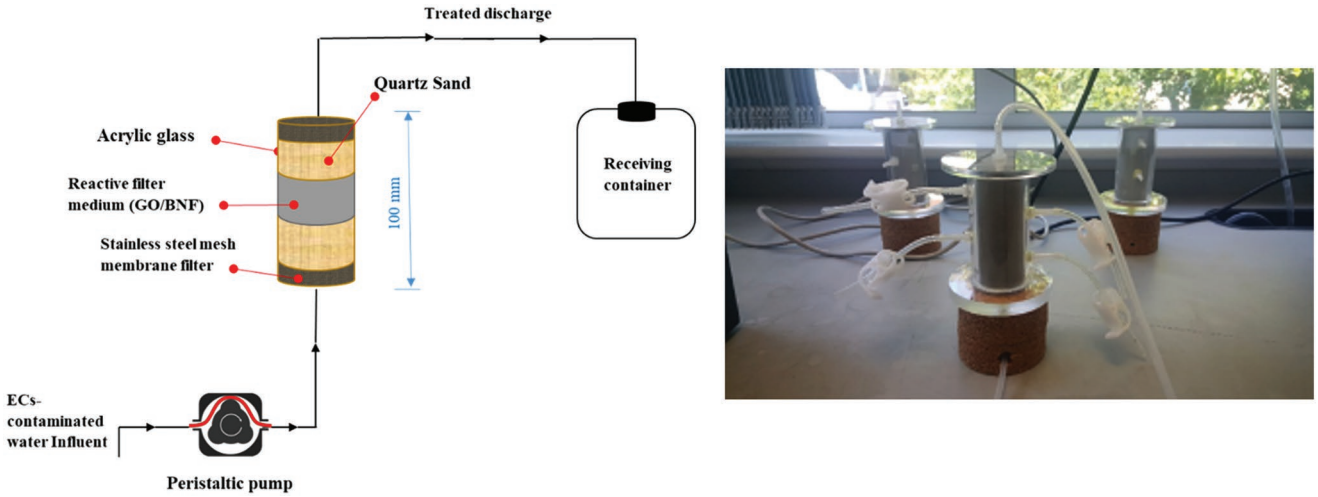

Figure 1. Schematic diagram for column filter setup (left) and a photo of 40 mm ID adsorption column filter (right).

sand, and all the slurry was added. The column filter was then fully run through for at least two hours with deionized water for washing. The test temperature was maintained at room temperature, and the solutions were covered to protect them from photolysis. The peristaltic pump was set to a flow rate of 0.5 mL min^{-1}. Contaminated solution passed through the base of the column through a grating, then was pumped through 10 cm of filter media up to the top plate, where it passed through another grate to the effluent tube. Sealing tape was required at the interface between the top "plate" and the main column body to provide an impermeable seal. Samples were taken periodically every half an hour within 10 h.

2.3.2. Column studies on GEM in drugs-contaminated water

Column filter tests were performed to quantitatively evaluate the efficacy of PG and GO0BNF materials as filter media to remove GEM from a mixture of six ECs (atenolol, carbamazepine, ciprofloxacin, diclofenac, gemfibrozil, and ibuprofen) from their mixed solutions in DW, SGW, and MWW matrices. The columns were made of acrylic glass with a height of 100 mm and an ID of 18 mm. They were covered with stainless steel mesh as a filter to prevent the particles from escaping out from them. A peristaltic pump was used to pump the pharmaceutical solution into the column in an up-flow mode from bottom to top. The column was filled with quartz sand. A stainless steel film (200 mesh) was applied to seal the column and prevent quartz sand from flowing into the solution after filtration. The top of the column was covered with seal tape to prevent leakage. Two columns were designed and set up. One was fully filled with sand, packed with sonicated PG suspension (5 g L^{-1}, 100 mg-PG), and the other was filled with sand and an intermediate filling of sand and sonicated GO/BNF suspension containing the adsorbent material (100 mg). All the columns were filled with sand by the wet-packing method.

In the column tests, the three columns were washed simultaneously with deionized water at a high pumping speed (30 rpm). Then, the speed of the peristaltic pump was adjusted to 3 rpm (0.5 mL min^{-1}), and the column test was completed in 5 h. The samples (3 mL) were taken from the discharge every 30 min for further examination. The concentration of the prepared pharmaceutical solutions was 1 mg L^{-1} for each EC. The tests were divided into three groups using DW, SGW, and MWW, respectively.

2.4. Characterization

Phase composition of the NGP raw material and the test samples (GO, BNF, and GO/BNF) were determined based on X-ray diffraction (XRD) analysis (D8 advanced, Bruker) within a range of 10–80° (2θ) at a scan rate of 5° min^{-1} (2θ). Morphologies of as-prepared samples were examined using a high resolution scanning electronic microscope (FESEM) (TESCAN VEGA3 SEM) and a transmission electronic microscope (TEM, JEOL-2100), both of which were linked with an energy-dispersive X-ray spectroscope (EDS). To improve their electrical conductivity, all the samples were mounted onto conductive carbon adhesive tapes and surface gold-coated before subjection to SEM examination. For the Fourier-transform infrared spectroscopy (FT-IR, Bruker Optics Tensor-27), infrared (IR) absorbance spectra were recorded between 500 and 4000 cm^{-1} at a resolution of 4 cm^{-1} using 20 coadded scans. Material particles (5 mg) and potassium bromide (KBr, 180 mg) were thoroughly mixed in an agate mortar, and then the mixture was pressed under a pressure of 5 tons for 2 min to form a pellet. Each pellet was placed in an attachment and then analyzed in the optical compartment of the FT-IR. A UV–vis absorption spectrophotometer was used to measure GEM sample concentrations at 220 nm. In addition, the samples of lower concentrations (below 1 mg L^{-1}) were examined using a liquid chromatograph (LC) equipped with a mass selective (MS) detector. A quantitative analysis of the pharmaceutical drug was performed using an Agilent 6420B triple quadrupole (QQQ) mass spectrometer (Agilent Technologies, Palo Alto, USA) hyphenated to a 1200 series rapid resolution HPLC system. The sample (5 µL) was loaded onto an Eclipse Plus C18 3.5 µm, 2.1 × 150 mm reverse-phase

analytical column (Agilent Technologies, Palo Alto, USA). The specific surface area and pore size of the tested samples were measured by the N_2 adsorption Brunauer-Emmett-Teller (BET) method. The nitrogen gas sorption analysis was carried out using a Quantachrome Autosorb-iQ gas area characterization analyzer. The samples were heated to 473 K under vacuum for 4 h to remove any contaminants inside the pores before cooling in an external bath to 77 K. The density of the foam was determined by measuring its mass and volume (the theoretical density of BN is 2.25 g cm^{-3}). Compression tests were carried out at a constant loading rate of 0.5 mm min^{-1} using an EZ20 Universal Material Testing Machine, Lloyd Instruments Ltd., UK.

The removal efficiency (R_t) of the adsorbed EC was calculated according to the following Equation (1) (where C_0 and C_t (mg L^{-1}) are the concentrations of GEM contaminants at the initial time and time*t*, respectively):

$$R_t = \frac{(C_0 - C_t)}{C_0} \times 100\% \quad (1)$$

The equilibrium amount of the adsorbed EC in the solid phase (Q_e, mg g^{-1}) was calculated according to the following Equation (2) (where C_0 and C_e (mg L^{-1}) are the initial and equilibrium concentrations of ECs, respectively; V(L) is the volume of the synthetic aqueous solution contaminated with GEM; and M(g) is the mass of adsorbent particles used):

$$Q_e = \frac{(C_0 - C_e)V}{M} \quad (2)$$

2.5. Modeling

As well documented in the literature, developing numerical models to simulate the reactive flow of contaminants within a porous medium is an efficient way to predict the pathways of solute transport through reactive materials.[18] Several studies utilized the data from lab-scale packed column tests to simulate the advection-dispersion-retardation flow through the porous medium, in which good correlation was achieved.[19] Moreover, predicting the effects of the relevant parameters in such models entails performing a thorough sensitivity analysis. Hence, it is crucial to develop such models to improve the preliminary design of the permeable reactive barriers (PRBs) and adsorption column filters as promising in situ techniques for groundwater and wastewater treatments, respectively.

1D solute transport model was developed to simulate the reactive flow of GEM through the designated reactive filter medium of GO/BNF. Hence, the well-known differential equation of advection-dispersion-retardation, Equation (3), was utilized in simulating such phenomena within the conducted column experiment:[19c,20]

$$R\frac{\partial C}{\partial t} = D_L\frac{\partial^2 C}{\partial x^2} - v\frac{\partial C}{\partial x} \quad (3)$$

where C is the GEM concentration (mg L^{-1}), t time (h), x the transport distance (cm), D_L the longitudinal coefficient of dispersion (cm^2 h^{-1}), v the average pore water velocity in the flow direction (cm h^{-1}), and R the factor of the GEM plume retardation within the column. R, in the present work, was estimated based on the equation of retardation term (Equation 4), which was derived from the nonlinear form of Langmuir isotherm (the best fitting isotherm model based on the sorption experimental results).[21]

Table 1. Column experimental conditions.

Parameter	Description	Value	Unit
L	Column length	4	Cm
d	Column diameter	10	Cm
A	Cross-sectional area of the column	12.564	cm^2
n_{GF}	GO/BNF porosity	0.98	–
n_s	Quartz sand porosity	0.386	–
γ_{GF}	GO/BNF density	0.033	g cm^{-3}
γ_s	Quartz sand density	1.014	g cm^{-3}
C_o	Initial concentration of GEM influent	10.5	mg L^{-1}
pH	–	(7 ± 0.5)	–
Q	Influent flow rate	0.5 (upward)	mL min^{-1}

$$R = 1 + \left(\frac{\gamma_b}{n}\right)\left[\frac{k_L S}{(1 + k_L C)^2}\right] \quad (4)$$

where γ_b is the material density of the porous media (g cm^{-3}), n the effective porosity of the porous media, k_L Langmuir isotherm constant (L g^{-1}), and S the maximum sorption capacity of the porous media towards GEM (mg g^{-1}). The values of all the above-mentioned parameters were estimated based on the data from the batch experiments on the removal of GEM by either GO/BNF or quartz sand. Hence, the values changed with respect to the porous media material corresponding to the column configuration.

All the parameters involved in the column tests, along with the initial and operating conditions, are summarized in **Table 1**.

The average values of pore water velocity in quartz sand and GO/BNF layers were calculated based on the well-known Darcy's formula:[22]

$$v = \frac{k\,i}{n},\ I = \frac{\Delta h}{L} \quad (5)$$

where k is the hydraulic conductivity of the porous medium material (cm h^{-1}), i the hydraulic gradient, and Δh the loss in the hydraulic head (cm) along a specific length (L) within the column (cm).

The longitudinal dispersion coefficient (D_L) was estimated based on the values of the dynamic dispersivity (α) in cm, and the effective molecular diffusion coefficient (D_e) in cm^2 h^{-1} (Equation 6). For a more accurate estimation of this term, the calculations included the tortuosity (tt), porosity (n), and molecular diffusion (D_m) effects, as important factors which influence the diffusion phenomena (Equation 7).

$$D_L = \alpha v + D_e \quad (6)$$

$$D_e = n\,tt\,D_m \quad (7)$$

Table 2. Calculated advection-dispersion parameters and the corresponding model stability indices.

Parameter	Description	Value	Unit
v_s	Average pore water velocity in quartz sand	4.9	cm h^{-1}
v_{GF}	Average pore water velocity in GO/BNF	6.65	cm h^{-1}
D_{Ls}	Longitudinal dispersion coefficient in quartz sand	9.99	cm^2 h^{-1}
D_{LGF}	Longitudinal dispersion coefficient in GO/BNF	868.422	cm^2 h^{-1}
α	Dynamic dispersivity	1.3	Cm
CFL_s	Courant–Friedrichs–Lewy number for quartz sand layers discretization	0.0049	–
CFL_{GF}	Courant–Friedrichs–Lewy number for GO/BNF layer discretization	0.0066	–
GN_s	Grid number for quartz sand layers discretization	0.490	–
GN_{GF}	Grid number for GO/BNF layer discretization	0.007	–

Table S5 (Supporting Information) displays all the considered formulas in the estimation of the average pore water velocity, dispersion coefficient, and their related parameters.

Numerical MATLAB code was developed, based on finite difference approximations, to solve the advection-dispersion-retardation equation, using the Crank-Nicolson approach.[23] Hence, Taylor series expansions were applied through replacing first-, second-order distance index derivatives, and first-order time index derivative by the first, second central, and first forward approximate differences, respectively. The total length of the column was distributed to nodes with a total number of 10, with the same column configuration as the experimental set up. The developed numerical code was used to determine the solution for all the time steps (over 10 h maximum time) along the column nodes. Such model discretization was selected to meet the minimum criteria of stability and accuracy of two factors, Courant–Friedrichs–Lewy (CFL) number and grid number (GN), represented by the following equations:[24]

$$\mathrm{CFL} = \frac{v\Delta t}{\Delta x} \leq 1 \tag{8}$$

$$\mathrm{GN} = \frac{v\Delta x}{D_L} \leq 2 \tag{9}$$

where Δt (0.001 h) and Δx (1.0 cm) are the designated time and distance steps according to the above-mentioned discretization, respectively. Consequently, the calculated values of the transport parameters (v and D_L) were utilized for the assessment of the model stability. **Table 2** shows the calculated values of the advection-dispersion parameters in sand and GO/BNF layers, as well as the corresponding values of the stability indices. The stability of the model was confirmed by the resulted very low values (≤1) of CFL, and reasonable values (≤2) of GN, with respect to the chosen discretization of the reactive domain.

3. Results and Discussion

3.1. Composition and Microstructure of GBM Sample

The crystal structure of graphene-based materials was analyzed using X-ray diffractometer. **Figure 2** shows XRD patterns of NGP and GO materials and the samples (BNF and GO/BNF) prepared at 1423 K for 3 h. The XRD pattern of the as-received NGPs revealed sharp diffraction peaks at 26.35° and 44.26° (2θ), corresponding to the characteristic planes (002) and (100) of GNPs, respectively, along with a sharp diffraction peak at 54.35° (2θ) corresponding to the plane (004) of graphitic carbon.[7a] Graphite was identified in the NGP powder, suggesting that it was essentially very thin multilayered graphite. As for the synthesized GO powder, the diffraction peak located at 12.6° (2θ) confirmed the presence of GO phase.[4b] The diffraction peaks (2θ) found in the XRD pattern of BNF at 26.5° and 43.6° corresponded respectively to the (002) and (101) planes of BN; however, they were relatively low.[25] For the final GO/BNF sample, the phase composition was almost the same as the BNF, suggesting that the crystallinity of BN formed under the current nitriding condition and GO content was very low. Moreover, the density and compressive strength of the as-prepared GO/BNF and BNF samples were determined as 32–35 mg cm^{-3} and 40–47 kPa (GO/BNF) and 26–31 mg cm^{-3} and 25–30 kPa (BNF), respectively. These measurement results revealed the positive effect of introducing a small amount of GO on the mechanical properties of the foams.

The morphology features of as-prepared GO/BNF samples were examined using SEM and TEM. Microstructures of these samples synthesized at 1423 K for 3 h are shown in **Figure 3**. After foam-gel casting and nitriding, in the as-obtained GO/BNF sample, the banded structure with a width of 1–2 µm intertwined to form a foam skeleton, at the same time a small amount of GO connected with ribbon-shaped BN can still be seen (Figure 3a). The formation of these ribbon-shaped BN (Figure 3b) can be attributed to the ribbon-shaped precursor

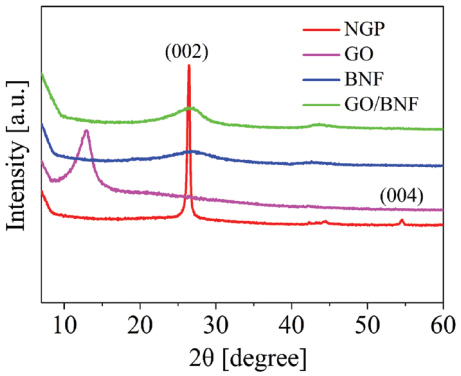

Figure 2. XRD patterns of NGP and GO materials and GO/BNF and BNF samples prepared at 1423 K for 3 h.

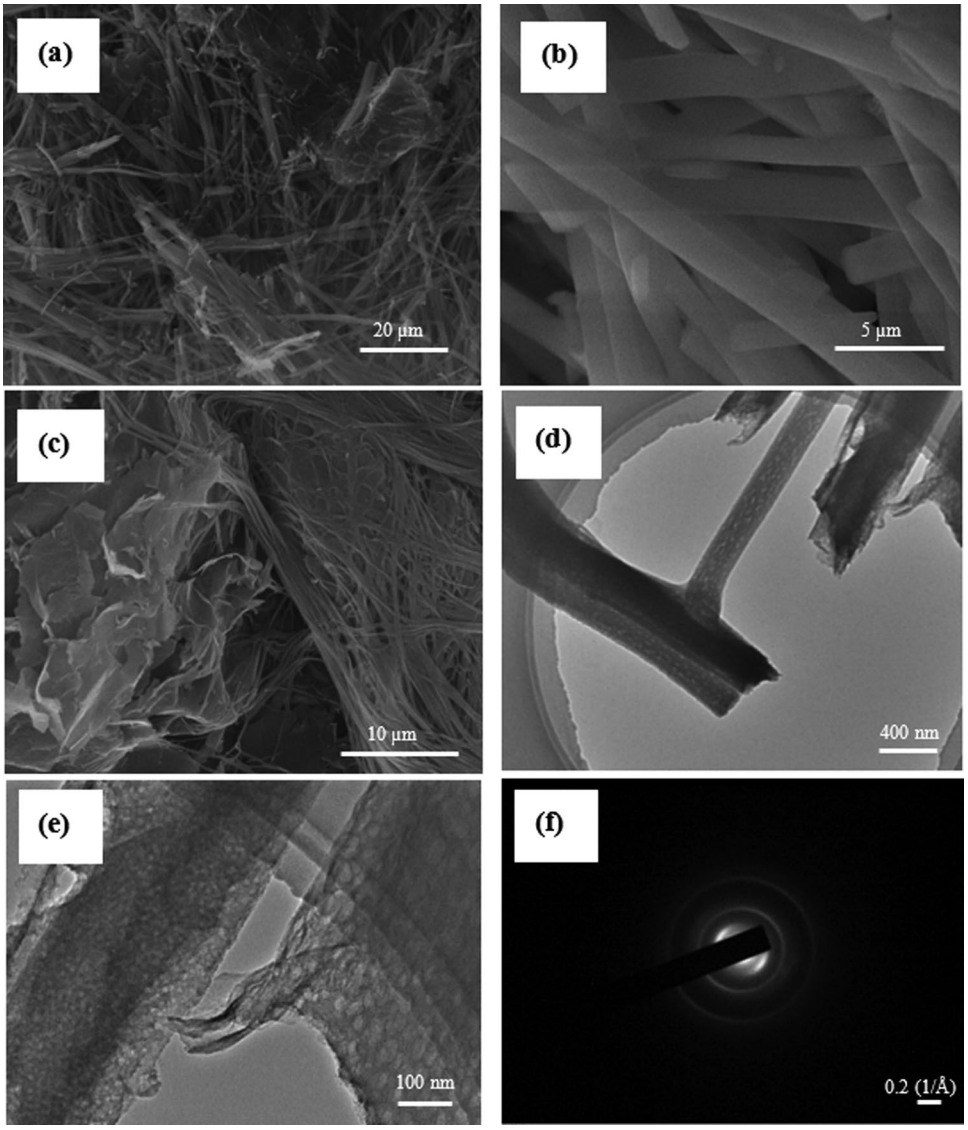

Figure 3. a–c) SEM and d–f) high-resolution TEM images of GO/BNF prepared at 1423 K for 3 h.

formed by the hydrogen bond interaction between melamine and boric acid during the gelation process. These band-shaped precursors provided some strength for the green samples and final foams, maintaining a complete framework structure at a very low solid content of 4.67 wt% (Figure 3c).

It can be seen that the width of the band structure generated in the sample was about 400–500 nm in width and about a few microns in length (Figure 3d). There were many mesoporous structures with diameters of 10–40 nm, on the surface of the band structure. It is believed that the band-shaped and flake phases were BN and GO (or reduced GO sheets shown in Figure 3e due to high temperature reduction), respectively. The selected area electron diffraction pattern (SAED) (Figure 3f) shows that the ribbons had an amorphous structure, which is consistent with the XRD results (in Figure 2). The formation of these structures increased the specific surface area of the final GO/BNF sample to a certain extent, thereby improving its adsorption performance.

3.2. Adsorption Properties of GBM Sample

Batch tests were conducted for different contact times to acquire kinetic profiles for the GEM contaminant adsorption onto NGP, BNF, and GO/BNF (**Figure 4**). Fast sorption kinetics or removal efficiency was observed in the initial stage of adsorption (5 min) for GO/BNF. However, the adsorption extents in the cases of using NGP and BNF were relatively low. With increasing the time, the removal in the case of using NGP initially increased but later started to decrease, indicating that the adsorption rate of the adsorbent for GEM was fast, but the adsorption was not firm. On the other hand, with increasing the adsorption time, the removal rate in the case of the control sample using BNF slightly increased, indicating the overall outperformance of GO/BNF, achieving a removal efficiency of GEM contaminants of >90% in 10 min. Moreover, GO/BNF foams were found to be highly efficient for GEM contaminants removal in considerably low dosage (250 mg L^{-1}). The

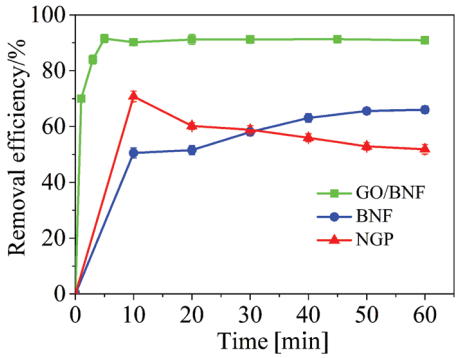

Figure 4. Effect of contact time on adsorption of GEM onto NGP, BNF, and GO-BNF. Error bars were calculated based on standard deviation values (C_0 = 10.5 mg L^{-1}; adsorbent dosage: 250 mg L^{-1}; room temperature: 295 ± 3 K).

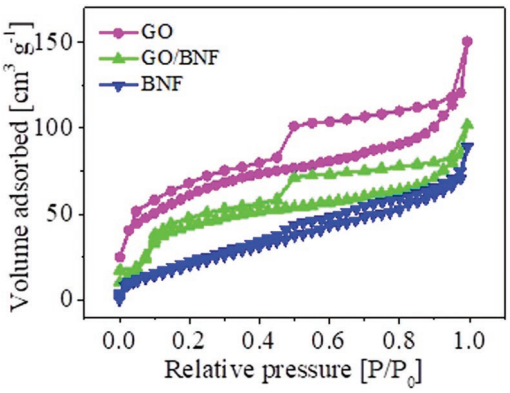

Figure 5. Nitrogen adsorption–desorption isotherms profiles of GO/BNF and BNF synthesized at 1423 K for 3 h.

applied dosage was significantly lower than that applied to efficient pharmaceutical decontamination in previous studies, involving treatment using activated carbon (e.g., 3000 mg L^{-1} on average[26] and above 5000 mg L^{-1}[27]).

To illustrate the sorption mechanism and the effect of surface area, nitrogen sorption isotherms of as-obtained GO powder, GO/BNF and the BNF control sample are given in **Figure 5**, showing that their BET specific surface area was respectively 221.9, 117.8, and 88.7 m^2 g^{-1}. The considerably higher surface area of GO/BNF is believed to arise from the flake-like morphology and relatively high surface area of GO.

Furthermore, adsorption capacities of as-prepared GO/BNF and BNF for GEM contaminants were examined, and the adsorption isotherms were simulated using the following linear forms of Langmuir (Equation 10) and Freundlich models (Equation 11):

$$\text{Langmuir}\ \frac{C_e}{Q_e} = \frac{1}{Q_e K_L} + \frac{C_e}{Q_s} \tag{10}$$

$$\text{Freundlich}\ \ln Q_e = \frac{1}{n}\ln C_e + \ln K_F \tag{11}$$

where K_F (mg g^{-1}) is the Freundlich constant, i.e., coefficient of adsorption capacity, and n the adsorption intensity constant (calculated from the ln C_e versus ln Q_e plot). Q_s (mg g^{-1}) is the maximum (saturation) adsorption capacity at the monolayer coverage, and K_L (L mg^{-1}) the coefficient of the energy of adsorption that shows the affinity of the binding sites.

The adsorption parameters, correlation coefficient (R^2) and the normalized adsorption capacities of BNF and GO/BNF foams obtained by the Langmuir and Freundlich model fitting and calculation are shown in **Figure 6** and **Table 3**, respectively (where the normalized adsorption capacity refers to the ratio of the maximum adsorption capacity to the specific surface area). The correlation coefficients R^2 of BNF and GO/BNF samples fitted by the Langmuir model are 0.998 and 0.993, respectively. Therefore, it can be inferred that the Langmuir model is more suitable for the study of pharmaceutical GEM adsorption by BN-based foam. In addition, the maximum adsorption capacity of GO/BNF (55.1 mg g^{-1}) was about 37% higher than that of BNF (40.9 mg g^{-1}), and the normalized adsorption capacity was also 4% higher (0.47 vs 0.45 mg m^{-2}). The reason can be attributed to the co-adsorption effect of GO and BN. The maximum adsorption capacity of GO for GEM (34 mg g^{-1}) was reported by us elsewhere, along with the results of adsorption equilibrium, kinetics, thermodynamics, pH and temperature effects, and reusability studies on GEM sorption onto GO.[4b]

Table 4 compares GEM adsorption performance between GO/BNF, BNF, and other adsorbents found in the literature. Compared with the Fe_3O_4 coated polymer clay composite, the BNF sample had a slightly lower specific surface area, while its adsorption capacity and normalized adsorption capacity were around 65% and 73% higher, respectively.[28] It can be seen that the specific surface area of the GO/BNF was relatively higher than that of Fe_3O_4 coated polymer clay composite (≈24%), and

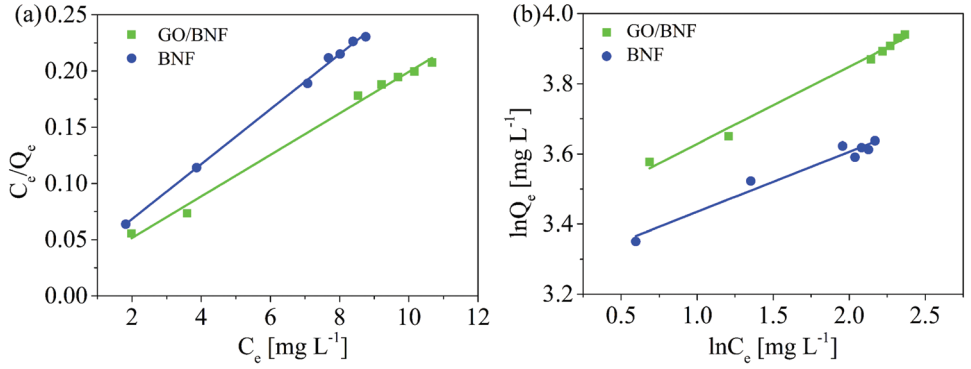

Figure 6. a) Langmuir adsorption isotherms and b) Freundlich adsorption isotherms of GEM degradation by as-prepared GO/BNF and BNF foams.

Table 3. Equilibrium parameters and normalized adsorption capacity for the adsorption of GEM onto GO/BNF and BNF foams.

	Langmuir			Freundlich			
Experiment	q_e [mg g^{-1}]	K_L [L mg^{-1}]	R^2	n	q_e [mg g^{-1}]	R^2	Normalized adsorption capacity [mg m^{-2}]
GO/BNF	55.1	1.262	0.993	34.63	51.4	0.985	0.47
BNF	40.2	1.258	0.998	26.14	40.1	0.956	0.45

its adsorption capacity and the normalized adsorption capacity were respectively 2.2 and 1.8 times as high as in the case of Fe_3O_4 coated polymer clay composite. With respect to the data reported in the literature,[28] the normalized adsorption capacity values of GO/BNF and BNF foams were relatively higher, along with other advantages, such as simple synthesis process, environmental friendliness, and easy recycling of 3-D blocks.[30] Furthermore, the as-prepared foams (117.8 m^2 g^{-1}, 55.1 mg g^{-1}) possessed GEM adsorption capacity greatly higher than that of the two other clay materials in Table 4 (vermiculite (0.08 mg g^{-1}) and LECA (0.015 mg g^{-1})). This indicates that inorganic clay materials have a poor affinity for organic GEM pharmaceuticals. In comparison, the foam composite could readily adsorb GEM, attributing this to the selective adsorption capability of GO and BN for GEM and the addition of GO (organic material) that further promoted the adsorptive property of the inorganic foam base (BN). For comparison, porous graphene was examined in the same batch tests and the results were in accordance with those reported previously.[4b] It had the largest specific surface area and slightly lower adsorption capacity (the lowest normalized adsorption capacity, Table 4). The removal rate of GEM by GO/BNF was the highest among all the tested graphene-based materials (GO and PG), i.e., the fastest adsorption kinetics, as illustrated in Figure S1 (Supporting Information). To sum up, the porous GO/BNF and BNF prepared by the method developed in this work had a relatively high maximum adsorption capacity and a normalized adsorption capacity for GEM, indicating that they had better absorption and removal performance for pharmaceutical GEM.

A recyclability test was carried out to demonstrate the reusability of GO/BNF and BNF. The GO/BNF and BNF were recycled several times after regeneration via a suction filter, followed by repeated washing with deionized water, and 4 h drying at 383 K. **Figure 7** illustrates the recyclability of GO/BNF and BNF in the GEM uptake process. The GO/BNF showed reasonable GEM removal capabilities after several cycles without suffering any major loss in sorption. In these cycles, the removal efficiency appeared to be decreased slightly, which was most likely due to an incomplete regeneration process as well as some adsorbent mass loss arising from the adhesion of some of the particles to surfaces of some tools (flasks, funnels, etc.) and filter paper during the repeated suction filtration, washing, and drying processes of GO/BNF and BNF foams. Even so, as can be seen from Figure 7, after four (BNF) or five (GO/BNF) consecutive adsorption-desorption cycles, the removal efficiency of GEM still remained as high as about 75% of the original one.

3.3. Adsorption Mechanism of As-Prepared Samples

A plausible mechanism of GEM adsorption by the graphene-based composite foam can be described in terms of chemisorption. The adsorption equilibrium of GEM by the foam material followed the Langmuir isotherm model, as indicated by the high values of correlation coefficients (Section 3.2). The Langmuir isotherm is generally a proper model for depicting a chemical adsorption process in which the adsorbent and adsorbate form ionic or covalent chemical bonds between their reactive groups.[31] Besides, the kinetic data were well fitted to the pseudo-second-order kinetic model, which supports the chemisorption hypothesis.

XRD results (**Figure 8**) showed that there was no obvious change in the foam material's crystal structure or composition. The XRD patterns of adsorbents (GO, BNF, GO/BNF) before adsorption (Figure 2) were typical of those shown by (spent) adsorbents after GEM adsorption. Obviously, GO and GO-GEM (i.e., GO after GEM adsorption) showed their characteristic peak at 12.6°. In comparison, both BNF-GEM and GO/BNF-GEM demonstrated shorter and broader peaks, revealing the amorphous structure, as additionally verified by SAED (Figure 3f). Accordingly, amorphous BN was the dominant phase, while detected h-BN (hexagonal form) showed a diffraction peak at 26.3° (highlighting (002) reflection) and another broad peak at 40–45° corresponding to the unresolved reflections (100) and (101), which characterizes the layered hexagonal structure of bulk BN. GO's (or rGO's) characteristic peak was absent from the XRD pattern, most likely due to the very low graphene content. On contrary, the XRD pattern of the pure GEM drug showed its crystalline nature.

Table 4. Comparison of maximum adsorption capacities of GEM by various adsorbents (NA: not available).

Adsorbent	S_{BET} [m^2 g^{-1}]	Adsorption capacity [mg g^{-1}]	Normalized adsorption capacity [mg m^{-2}]	Refs.
Fe_3O_4 coated polymer clay composite	94.81	24.79	0.26	[28]
Light expanded clay aggregates (LECA)	NA	0.015	–	[29]
Exfoliated vermiculite	NA	0.08	–	[29]
Porous graphene powder	670	40	0.06	[4b]
BNF porous ceramics	88.7	40.9	0.45	This work
GO/BNF	117.8	55.1	0.47	This work

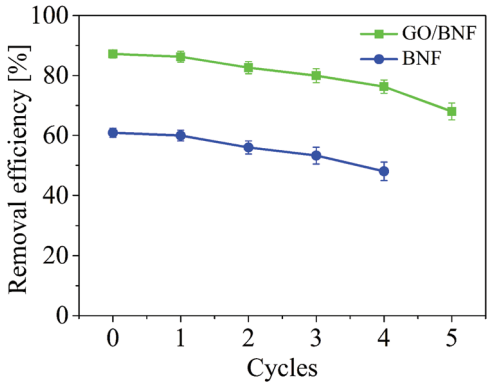

Figure 7. Adsorption cycles of GO/BNF and BNF porous ceramics on GEM.

Adsorption mechanism is further scrutinized by FTIR analysis. The infrared spectra of the GEM drug and both BNF-supported GO pre- and post-GEM adsorption are presented in **Figure 9**. Bands of infrared spectra were detected at 1705.8, 1127.2, and 1166 cm^{-1}, corresponding to C—O stretching vibrations, which are the characteristic infrared spectra of gemfibrozil ($C_{15}H_{22}O_3$).[32] In the case of GO/BNF, BN vibrations in the h-BN nanosheets appeared at 810.1, 1394.53, and 3437.15 cm^{-1}. Usually, h-BN shows clear and distinguishable absorption peaks around 810 cm^{-1} and 1360 cm^{-1}, related to the out-of-plane (bending vibration of B–N–B) and in-plane stretching vibrations of the B—N bond, respectively.[33] Also, toward around 1384 cm^{-1} peak, the phonon modes of turbostratic h-BN usually appear as in our case.[33b] On the other hand, FTIR pattern of GEM displayed characteristic bands of distinguishable functional groups: 1049.27, 1213.23, 1402.25 cm^{-1} (C—O stretching in epoxy group), 1708.9 cm^{-1} (C=C stretching in aromatic ring), 2611.1 cm–1 (C=O stretching in carboxylic acid), 2958.8 cm^{-1} (C—H stretching vibrations) and 3454.51 cm^{-1} (O—H stretching vibrations).[4b] The FTIR spectra of GO/BNF before and after GEM adsorption revealed that most of the peaks of GEM were not observed after GEM adsorption. However, small peak shifts occurred after GEM adsorption onto GO/BNF as characteristic bands shifted from 810 to 806.25 cm^{-1}, 1394.53 to 1382.96 cm^{-1}, and 3437.15 to

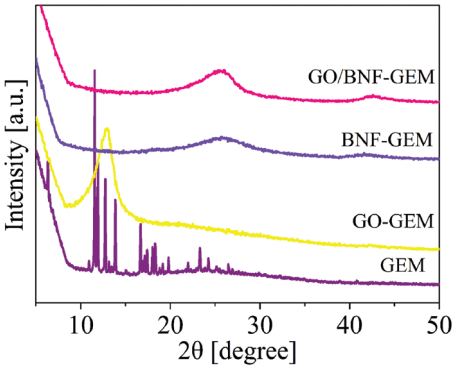

Figure 8. X-ray diffraction patterns of raw GEM pharmaceutical contaminants, GO, BNF, and GO/BNF before and after GEM adsorption (Adsorption conditions: 10.5 mg L^{-1} GEM solution, 250 mg L^{-1} GO, BNF, and GO/BNF dose).

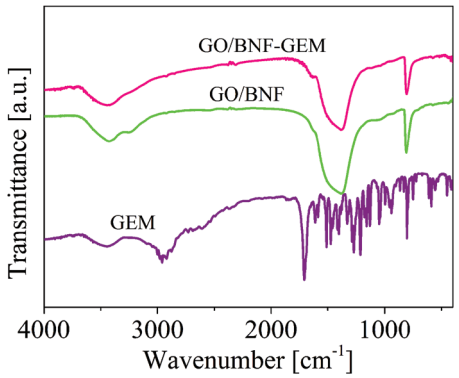

Figure 9. FT-IR spectra of GO/BNF before and after adsorption of the GEM pharmaceutical contaminants (adsorption conditions: 10.5 mg L^{-1} solution, 250 mg L^{-1} GO/BNF dose).

3444.87 cm^{-1}, indicating that the amount of the adsorbed GEM in comparison with that of the adsorbent was not so significant. Especially, BNF showed amorphous nature, and h-BNF hardly contributed to the adsorption.

The GO material in the final product foam should have been converted to reduced graphene oxide (rGO) or porous graphene (PG). As reported previously, GO can be reduced at a temperature above 350° to rGO, and the full elimination of OCFGs by thermal reduction is possible at an elevated temperature (>1000 °C) and a low pressure, which is close to the foam formation condition (1150 °C).[4b,34] Therefore, GEM adsorption onto thermally reduced GO part could be owed to physisorption that included hydrogen bonding, electrostatic and π–π interactions, and van der Waals forces.[4b]

3.4. Column Studies

3.4.1. Column Tests

GEM (10.5 mg L^{-1}) was removed from single solutions in DW background via filtration through 40 mm ID graphene-based adsorbent column filters. Two adsorbent materials, PG and GO/BNF, were compared in these column studies. The former was produced based on a facile synthesis process previously reported by us.[4b,7c]

S-shaped breakthrough curves are shown in **Figure 10**, illustrating the filtration performances of PG- and GO/BNF-based column filters. Bare dry PG layer showed no significant filtration performance, while the performance illustrated by the graph in Figure 10 was linked to sonicated PG mixed with/supported on sand particles (Section 2.3.1) for maximum functionality. A slightly better performance was achieved in the GO/BNF packed adsorption column filter due to the already available supporting property of BNF that segregated GO (or graphene) sheets. However, in both breakthrough concentration profiles (Figure 10), the concentration ratio (C_t/C_0) never approached unity. According to Babu et al., the increase in the mass transfer coefficient could cause the adsorbate removal ratio to reach a specific constant value (less than unity) and asymptotically befell constant after some time.[35] The higher the external mass transfer coefficient, the lesser value than

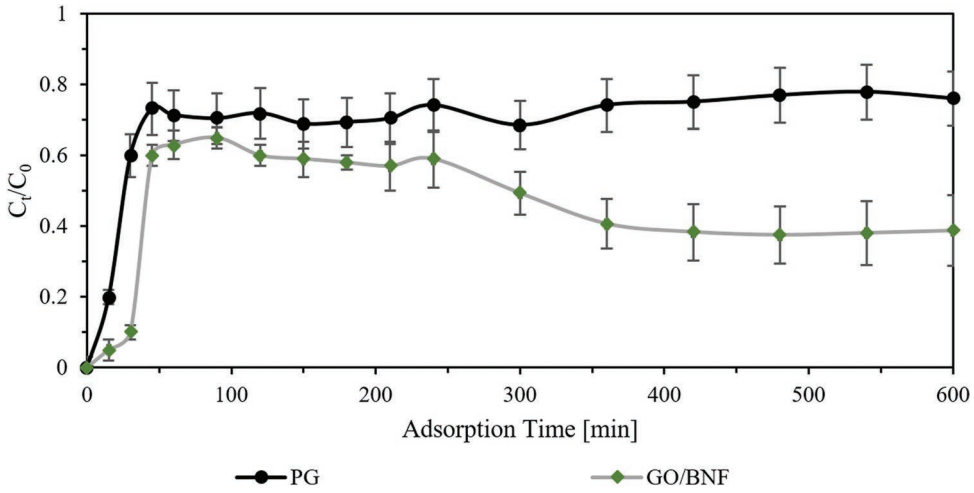

Figure 10. Filtration of GEM-contaminated DW through PG and GO/BNF packed filters.

unity asymptotically approached by the outlet concentration/initial concentration ratio. That seemed reasonable in the case of highly porous GO/BN foam containing >98% porosity, which consequently had a higher external mass transfer coefficient, and exhibited a lower asymptotic concentrations ratio line than that in the case of porous graphene.

3.4.2. Interference in Different Water Bodies

Three different water bodies (DW, SGW, and MWW) spiked with six pharmaceuticals (ATL, CBZ, CIP, DCF, and IBF), including the under-investigated contaminant GEM, were filtered through PG and GO/BNF media in the adsorption column tests. In these tests, both PG and foam were sonicated in suspensions, homogeneously mixed with sand and packed inside the 18 mm ID column filters. Both packing materials were subjected to the same treatment (i.e., sonication), unlike that in Section 3.4.1 in which the foam material was utilized in its bulk form without change in structure. The filtration results are presented in **Figure 11**. The performance of PG in DW and SGW was appreciable, reducing GEM contamination to trace concentration level for more than 200 min (Figure 11a), despite the presence of other five pharmaceuticals (in DW and SGW) and numerous interfering contaminants (in SGW, Table S3, Supporting Information). Contrarily, GO/BNF material performed less effectively in filtering DW contaminated with six pharmaceutical contaminants. Specifically, GEM concentration rose quickly and the breakpoint was noticeably early as shown in Figure 11a. However, the presence of SGW components enhanced the removal performance of foam material. As such improvement was not clearly witnessed in the case of PG, while the fact that SGW contaminants had no adverse interference with PG filtration performance in SGW, illustrating the enhancing effect. However, the negative interference imposed by ammonium and chloride competing ions degraded PG filtration performance in the case of MWW. Also, for the same reason, GO/BNF performed inefficiently in adsorbing the GEM contamination in MWW (Figure 11b).

The aforesaid results suggested that PG nanosheets sonicated and supported on the sand made their surface area (containing active sites) free and accessible to GEM molecules. The same phenomenon was witnessed using the unmodified GO/BN foam material. Once the foam material was subjected to sonication in suspension media, its structure was deteriorated and damaged as evidenced by Figure S2 (Supporting Information). Therefore, if applied directly without modification, the graphene-based foam material could be feasible for filtration systems for wastewater treatment. While concerns may be raised about the high synthesis temperature of GO/BNF, recent

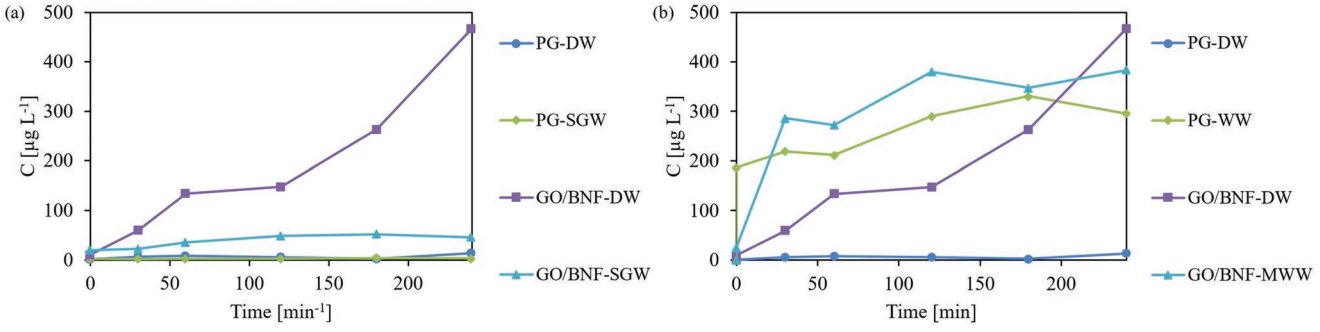

Figure 11. The breakthrough curves of GEM adsorption onto PG and GO/BNF in a) DW and SGW and b) DW and MWW as backgrounds (pH 7.5; initial individual GEM concentration: 1 mg L^{-1}; PG or GO/BNF loading dosage: 100 mg).

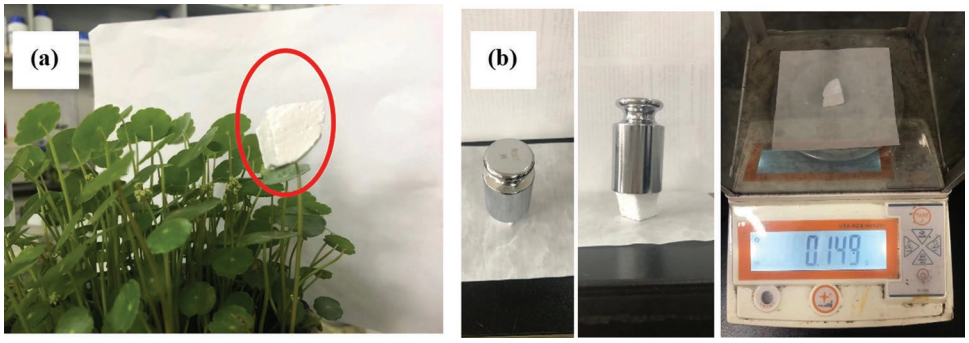

Figure 12. Demonstration of physical properties of the foam (lightness and strength): a) as-prepared foam placed on plant leaves, and b) the foam material withstanding a standard cylindrical weight of around 1340 times its own weight.

studies demonstrated that BNF could be produced at a lower temperature of around 650 °C.[36] In addition, in comparison with that of PG, the synthesis process of GO/BNF is simpler and more straightforward, without explosion risks, toxic material involvement, and toxic gases evolution. Additionally, the foam material demonstrated some appreciable physical characteristics such as low bulk density (light), high porosity (>98%), and considerable strength, as presented together in **Figure 12**.

3.4.3. Modeling

Modeling Results: A numerical model was developed to simulate the reactive solute transport of GEM influent through the GO/BNF filter. **Figure 13** compares modeling and experimental results of GEM concentration. The actual breakpoint time was earlier than that predicted by the model. This could be attributed to several reasons, including the small mass of the foam (100 mg), which was not enough to cover the whole cross-sectional area of the column filter. The coefficient of determination (R^2) was considered for evaluating the goodness of fit between the obtained results, suggesting a loose fit ($R^2 = 0.56$). Moreover, the diagonal error chart (**Figure 14**) indicated that approximately 60% of the comparison data were within the ±20% error range, corresponding to the diagonal correlation line (zero-error line). Such low correlation between model and experimental results was mainly attributed to the steep rise in the experimental values of GEM effluent concentration within the early hours of the experiment time (the first 2 h), followed by a fluctuation within the next 4 h. Meanwhile, modeling results showed a steady rise of GEM concentration to be stabilized after 4 h until the end of the experiment at 4.03 mg L^{-1}, with around 62% removal efficiency. Despite the good stability of the developed model, it could be anticipated that there are two factors which might cause such discrepancy in data trends of the solute transport within column experiments, either dispersion or retardation related factors, including v, D_L, and K_L. Hence, it was necessary to conduct sensitivity analysis of the model towards the change in such factors, as will be described and discussed in the following section.

Sensitivity Analysis: Sensitivity analysis was conducted to determine the most critical advection-dispersion-retardation parameters for the transport model. Hence, the sensitivity of the model is expressed by the variation in GEM effluent concentration with respect to the change in the values of the chosen parameters (v, D_L, and K_L), based on the following formula:[19c]

$$S = \frac{\Delta C}{\Delta p} \tag{12}$$

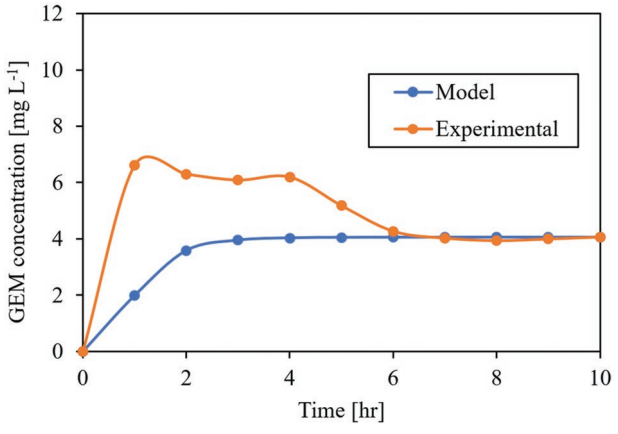

Figure 13. Experimental and model GEM effluent concentration.

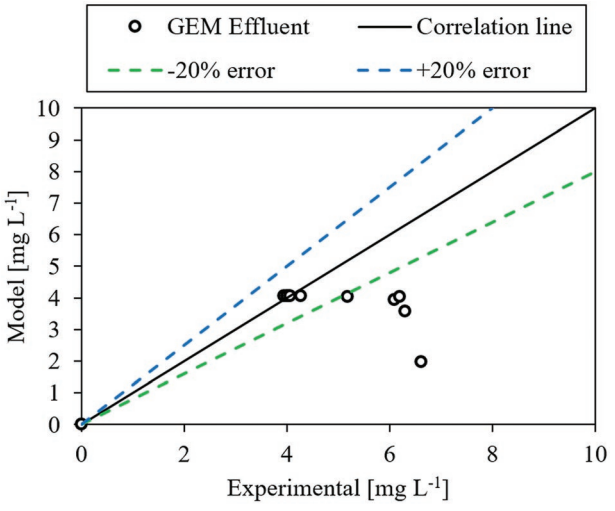

Figure 14. Diagonal error chart of experimental and model effluent results.

Table 5. Calculated advection-dispersion parameters and the corresponding model stability indices.

Parameter	Description	Base-line value	Variation range
v_s	Average pore water velocity in quartz sand	4.9 cm h^{-1}	±50%, 90%
v_{GF}	Average pore water velocity in GO/BNF	6.65 cm h^{-1}	±50%, 90%
D_{Ls}	Longitudinal dispersion coefficient in quartz sand	9.99 cm^2 h^{-1}	±50%, 70%
D_{LGF}	Longitudinal dispersion coefficient in GO/BNF	868.422 cm^2 h^{-1}	±10%, 15%
K_{Ls}	Langmuir isotherm constant of quartz sand	1262 L g^{-1}	±50%, 90%
K_{LGF}	Langmuir isotherm constant of GO/BNF	0.04 L g^{-1}	±50%, 90%

where S is the sensitivity index of the model to the change in the simulated GEM effluent concentration (ΔC), corresponding to the variation in parameter value (Δp). The baseline values and the chosen variation range of each parameter are presented in **Table 5**, calculated in this study (Section 2), and extracted from other reports.[4b,9,19c]

Sensitivity analysis results for the change in the simulated GEM effluent concentration with respect to the change in the selected parameters are shown in **Figure 15**. Moreover, sensitivity indices were plotted for the effluent concentration variation corresponding to the change in each parameter, with respect to time, as shown in **Figure 16**. Sensitivity index was

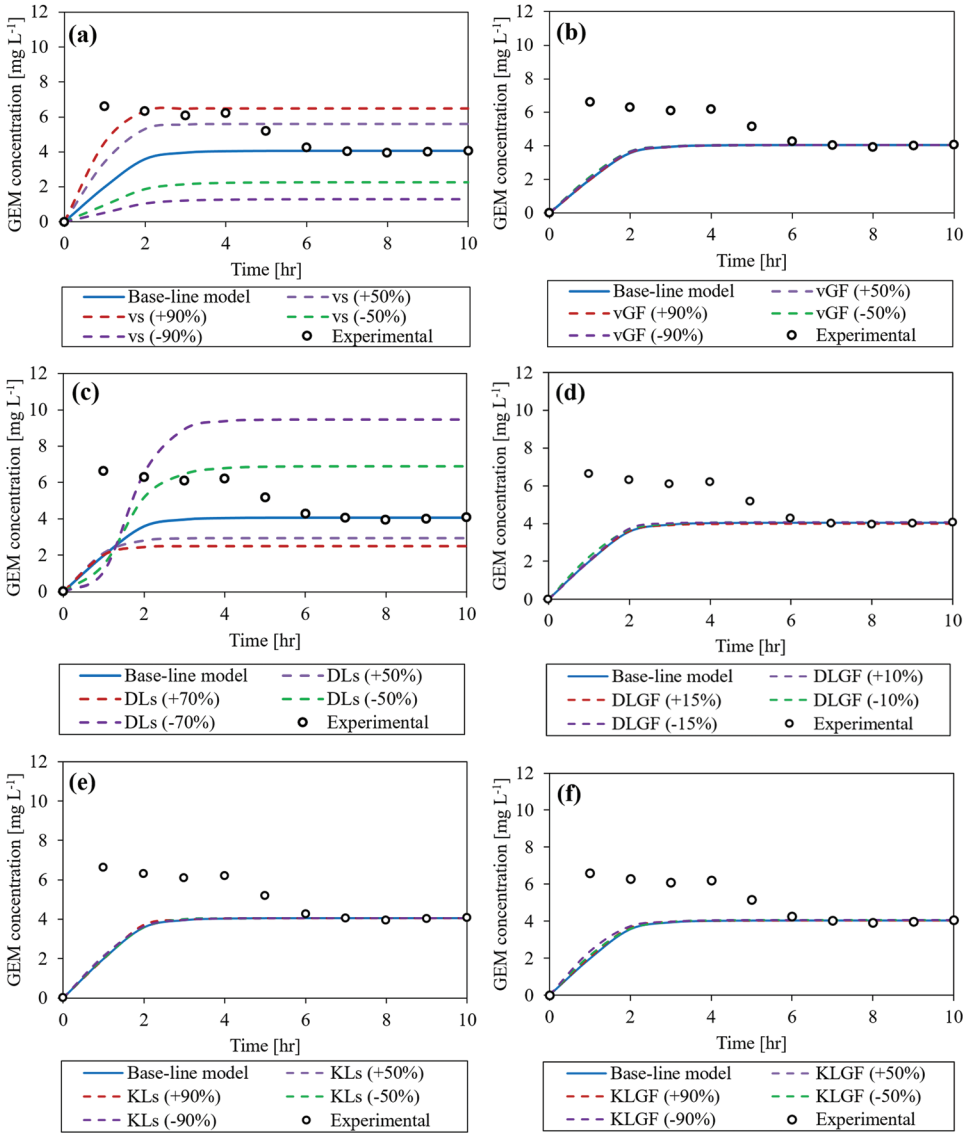

Figure 15. Sensitivity analysis of the simulated ECs effluent concentration to the change in: a) v_s, b) v_{GF}, c) D_{Ls}, d) D_{LGF}, e) K_{Ls}, and f) K_{LGF}.

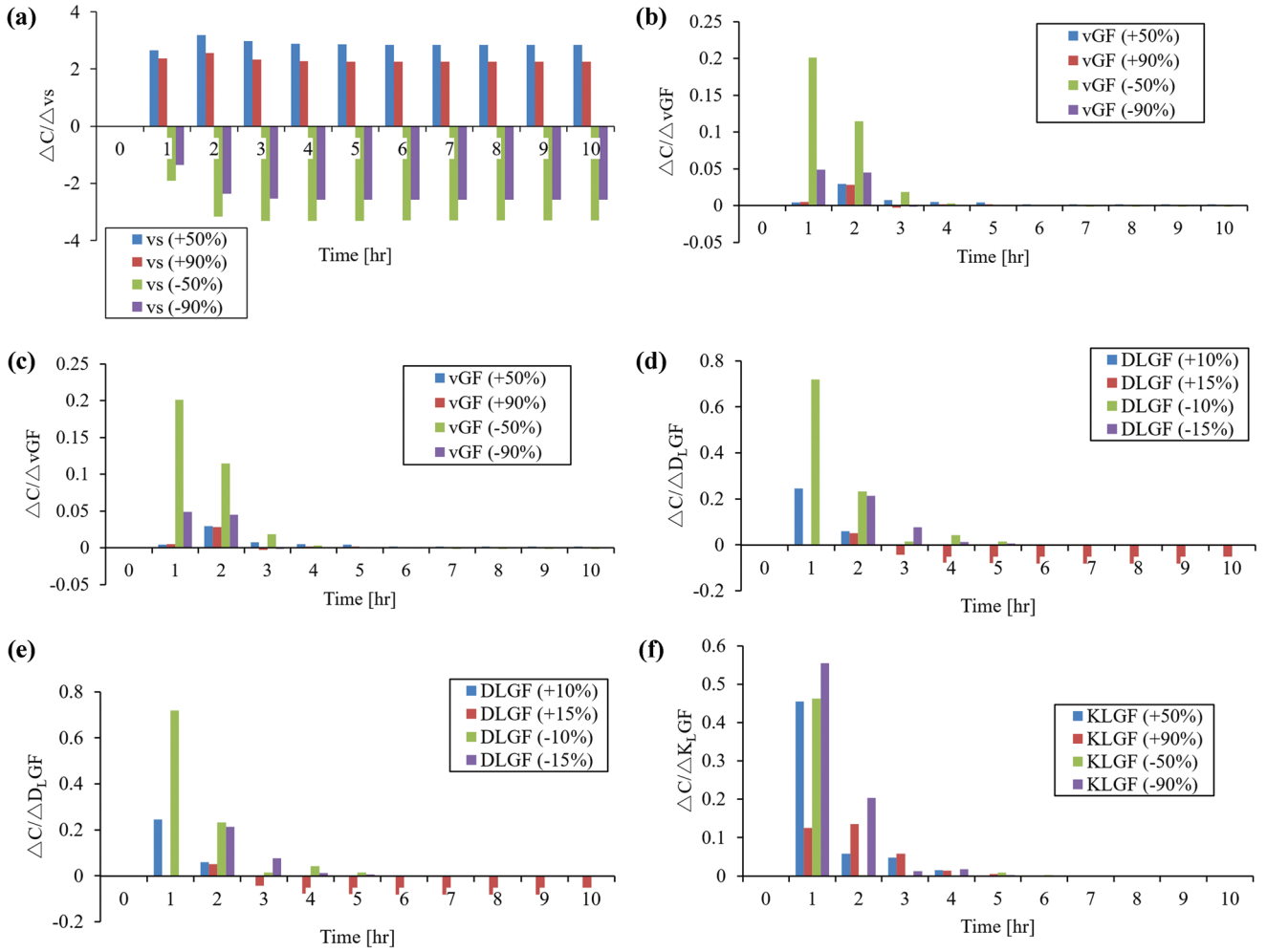

Figure 16. Sensitivity indices of the simulated ECs effluent concentration to the change in: a) ν_s, b) ν_{GF}, c) D_{Ls}, d) D_{LGF}, e) K_{Ls}, and f) K_{LGF}.

considered as an indicator for the criticality of each parameter towards the simulated solute transport model, where the high index value (regardless of the sign) of a specific parameter reflects the high sensitivity of the model to such parameter. Hence, it was clear that ν_s and D_{Ls} are most crucial parameters, corresponding to the highest values of sensitivity index, which reached 3.317(–) and 12.684(+), respectively. Moreover, the model is sensitive to some extent to the change in K_{Ls} with a maximum value of sensitivity index of 7.685(+). However, it has low sensitivity to the change in the advection-dispersion-retardation factors within the GO-BNF layer, including ν_{GF} and K_{LGF}, with maximum sensitivity index values of 0.201(+) and 0.554(+). On the correlation level, increasing ν_s by 90% and D_{Ls} by 70% resulted in the highest R^2 value of 0.69 and 0.74, respectively. It is worth mentioning that the low correlation between the experimental and the modeling results is mainly attributed to two reasons: 1) the early-stage fluctuation in GEM concentration in the experimental results of the column experiment, which is significantly hard to be simulated, and 2) the empirical assumption of the molecular diffusion factors, which has been reported previously in the literature to have a great effect on the breakthrough time.[37] Hence, it should be recommended to estimate the diffusion parameters for an accurate simulation of the experimental breakthrough data.

In order to better determine the effect of the most crucial model parameters on the trend of the solute transport model, an empirical curvature mapping was developed based on the sensitivity analysis results (Figure S3, Supporting Information). It was clear that ν_s has the widest effect zone by influencing the curvature of the effluent concentration profile at different sections and over long-time duration (2–10 h). Meanwhile, the parameters related to the reactive zone in the column (GO/BNF), including ν_{GF}, and D_{LGF} affected the curvature of the data trend but with different types of the impact, in terms of the intensity and the trend. Furthermore, D_{Ls} had an interesting influence on the curvature of the plotted data, via inversed trend of the impact with respect to changing the affected section of the curve.

Such results represented a great contribution to the research studies in this field, in terms of manipulating the preliminary design of the solute transport model parameters before moving to the scaled-up pilot installation of the column experiments. Moreover, the presented empirical curvature mapping would be very helpful in determining the most suitable parameters to be manipulated, thereby reducing the time-consuming trial experiments.

4. Conclusions

In this study, reduced porous graphene oxide nanosheets were successfully supported on ribbon-shaped boron nitride (BN) foam for the treatment of gemfibrozil (GEM)-contaminated water in batch tests and column studies. Compared with its graphene-based counterparts (such as graphene oxide (GO), porous graphene (PG), and nanographene platelets (NGP)), the graphene-based foam material showed distinctively fast adsorption kinetics towards GEM, with 90% removal efficiency in less than 5 min. In terms of durability, the foam-supported graphene-based nanomaterials exhibited a reliable GEM drug removal performance when reused for several cycles without any major loss in sorption. Also, the foam material showed impressive properties, such as lightness (≈33 Kg m^{-3} as bulk density) with a porosity over 98% and strength (≈44 kPa as compressive strength), and could endure 1300–1400 times its own weight. In filter applications, foam packed adsorption column filter outperformed sonicated PG nanosheets supported on the sand filter that treated GEM aqueous solutions. Numerical 1-D solute transport model was developed to simulate the experimental data of ECs removal within the GO/BNF filter medium. The selection of a suitable porous media material (either the packed column material or the reactive zone material), as well as the accurate experimental estimation of the advection-dispersion-retardation parameters are considerably crucial for the proper design and validation of the fixed-bed technology. Considering the above, the supported graphene-based composite foam for filter application would be a stepping stone to a great advancement in water and wastewater filtration technology. These findings suggest that highly porous foam-supported graphene nanomaterial filters with reduced contact times and longer breakthrough times could be readily produced for water and wastewater treatment. Finally, two major remarks should be made: the challenge of commercializing the proposed filter material will be overcome through progressive research innovation, and the actual remediation potential will be determined through pilot-plant studies, which are currently lacking in the literature.

Supporting Information

Supporting Information is available from the Wiley Online Library or from the author.

Acknowledgements

A.M.E.K. and L.H. contributed equally to this work. This work is part of the FAME (Fate and Management of Emerging Contaminants) Project, jointly funded by the Department of Science and Technology, Government of India (DST/TM/INDO-UK/2K17/66(C)) and the UK Natural Environment Research Council (NE/R003548/1) under India-UK Water Quality Programme.

Conflict of Interest

The authors declare no conflict of interest.

Data Availability Statement

The data that support the findings of this study are available in the supplementary material of this article.

Keywords

adsorption filters, foam, graphene-based materials, pharmaceutical contaminants, wastewater treatment

Received: January 12, 2022
Revised: April 28, 2022
Published online:

[1] a) L. Rizzo, C. Manaia, C. Merlin, T. Schwartz, C. Dagot, M. Ploy, I. Michael, D. Fatta-Kassinos, *Sci. Total Environ.* **2013**, *447*, 345; b) S. T. Ulu, *Chromatographia* **2006**, *64*, 447.
[2] C. Mimeault, A. Woodhouse, X.-S. Miao, C. Metcalfe, T. Moon, V. Trudeau, *Aquat. Toxicol.* **2005**, *73*, 44.
[3] M. Isidori, A. Nardelli, L. Pascarella, M. Rubino, A. Parrella, *Environ. Int.* **2007**, *33*, 635.
[4] a) E. C. Lima, *Ecotoxicol. Environ. Saf.* **2018**, *150*, 1; b) A. M. Khalil, F. A. Memon, T. A. Tabish, D. Salmon, S. Zhang, D. Butler, *Chem. Eng. J.* **2020**, *398*, 125440.
[5] a) A. M. Khalil, O. Eljamal, T. W. Amen, Y. Sugihara, N. Matsunaga, *Environ. Earth Sci.* **2018**, *77*, 489; b) C. Santhosh, V. Velmurugan, G. Jacob, S. K. Jeong, A. N. Grace, A. Bhatnagar, *Chem. Eng. J.* **2016**, *306*, 1116; c) S. Zhu, M. A. Khan, T. Kameda, H. Xu, F. Wang, M. Xia, T. Yoshioka, *J. Hazard. Mater.* **2022**, *426*, 128062.
[6] a) A. M. Khalil, O. Eljamal, B. B. Saha, N. Matsunaga, *Chemosphere* **2018**, *197*, 502; b) L. Zhao, J. Deng, P. Sun, J. Liu, Y. Ji, N. Nakada, Z. Qiao, H. Tanaka, Y. Yang, *Sci. Total Environ.* **2018**, *627*, 1253; c) A. M. Khalil, O. Eljamal, S. Jribi, N. Matsunaga, *Chem. Eng. J.* **2016**, *287*, 367; d) H. Xu, S. Zhu, M. Xia, F. Wang, X. Ju, *J. Hazard. Mater.* **2022**, *423*, 127192.
[7] a) L. A. Al-Khateeb, S. Almotiry, M. A. Salam, *Chem. Eng. J.* **2014**, *248*, 191; b) S. Zhu, Y.-g. Liu, S.-b. Liu, G.-m. Zeng, L.-h. Jiang, X.-f. Tan, L. Zhou, W. Zeng, T.-t. Li, C.-p. Yang, *Chemosphere* **2017**, *179*, 20; c) T. A. Tabish, F. A. Memon, D. E. Gomez, D. W. Horsell, S. Zhang, *Sci. Rep.* **2018**, *8*, 1817.
[8] a) P. R. Kidambi, D. Jang, J. C. Idrobo, M. S. Boutilier, L. Wang, J. Kong, R. Karnik, *Adv. Mater.* **2017**, *29*, 1700277; b) H. Chen, B. Gao, H. Li, *J. Hazard. Mater.* **2015**, *282*, 201; c) H. Xu, S. Zhu, M. Xia, F. Wang, *J. Hazard. Mater.* **2021**, *402*, 123815.
[9] A. M. Khalil, F. A. Memon, T. A. Tabish, B. Fenton, D. Salmon, S. Zhang, D. Butler, *Nanomaterials* **2021**, *11*, 79.
[10] a) X. Lu, A. Wei, Q. Fan, L. Wang, P. Chen, X. Dong, W. Huang, *Mater. Res. Bull.* **2012**, *47*, 4335; b) B. Y. Z. Hiew, L. Y. Lee, X. J. Lee, S. Thangalazhy-Gopakumar, S. Gan, S. S. Lim, G.-T. Pan, T. C.-K. Yang, W. S. Chiu, P. S. Khiew, *Process Saf. Environ. Prot.* **2018**, *116*, 262.
[11] J. Zhang, K. Ji, J. Chen, Y. Ding, Z. Dai, *J. Mater. Sci.* **2015**, *50*, 5371.
[12] a) H. Bi, X. Xie, K. Yin, Y. Zhou, S. Wan, L. He, F. Xu, F. Banhart, L. Sun, R. S. Ruoff, *Adv. Funct. Mater.* **2012**, *22*, 4421; b) H. Bi, X. Xie, K. Yin, Y. Zhou, S. Wan, R. S. Ruoff, L. Sun, *J. Mater. Chem. A* **2014**, *2*, 1652; c) L. Han, L. Huang, L. Dong, H. Zhang, Y. Pei, F. Li, Q. Jia, S. Zhang, *J. Am. Ceram. Soc.* **2020**, *103*, 5365.
[13] Y. Bi, L. Han, Y. Zheng, Y. Guan, H. Zhang, S. Ge, H. Wang, Q. Jia, Y. Zhang, S. Zhang, *ACS Appl. Mater. Interfaces* **2018**, *10*, 27416.
[14] L. Han, F. Li, X. Deng, J. Wang, H. Zhang, S. Zhang, *J. Eur. Ceram. Soc.* **2017**, *37*, 2717.

[15] a) S. Li, F. Liu, Y. Su, N. Shao, D. Yu, Y. Liu, W. Liu, Z. Zhang, *J. Hazard. Mater.* **2019**, *378*, 120669; b) J. Wang, D. Liu, Q. Li, C. Chen, Z. Chen, P. Song, J. Hao, Y. Li, S. Fakhrhoseini, M. Naebe, *ACS Nano* **2019**, *13*, 7860; c) Y. Xue, P. Dai, X. Jiang, X. Wang, C. Zhang, D. Tang, Q. Weng, X. Wang, A. Pakdel, C. Tang, *J. Mater. Chem. A* **2016**, *4*, 1469.
[16] a) I. Jauris, C. Matos, C. Saucier, E. Lima, A. Zarbin, S. Fagan, F. Machado, I. Zanella, *Phys. Chem. Chem. Phys.* **2016**, *18*, 1526; b) X. Zhu, D. C. Tsang, F. Chen, S. Li, X. Yang, *Environ. Technol.* **2015**, *36*, 3094.
[17] S. N. Abed, M. Scholz, *Environ. Technol.* **2016**, *37*, 1631.
[18] S. Banzhaf, K. H. Hebig, *Hydrol. Earth Syst. Sci. Discuss.* **2016**, *20*, 3719.
[19] a) C. Zhang, J. Zhang, S. Xu, H. Zhang, *Adv. Water Sci.* **2008**, *19*, 552; b) C. Yuan, T. Huang, X. Zhao, Y. Zhao, *Sustainability* **2020**, *12*, 3498; c) I. Maamoun, O. Eljamal, A. M. Khalil, Y. Sugihara, N. Matsunaga, *Transp. Porous Media* **2018**, *125*, 395.
[20] S. Mustafa, A. Bahar, Z. A. Aziz, S. Suratman, *J. Environ. Manage.* **2016**, *165*, 159.
[21] a) H. D. Sharma, K. R. Reddy, *Geoenvironmental Engineering: Site Remediation, Waste Containment, and Emerging Waste Management Technologies*, John Wiley & Sons, New York **2004**; b) S. E. Ingebritsen, W. E. Sanford, *Groundwater in Geologic Processes*, Cambridge University Press, Cambridge **1999**.
[22] C. H. Dix, *J. Geol.* **1971**, *79*, 505.
[23] M. M. Mortula, J. Abdalla, A. A. Ghadban, *Environ. Eng. Sci.* **2012**, *29*, 660.
[24] a) C. I. Steefel, K. T. MacQuarrie, *Rev. Mineral.* **1996**, *34*, 83; b) D. Schäfer, W. Schäfer, W. Kinzelbach, *J. Contam. Hydrol.* **1998**, *31*, 167.
[25] L. Han, A. M. Khalil, J. Wang, Y. Chen, F. Li, H. Chang, H. Zhang, X. Liu, G. Li, Q. Jia, *Sep. Purif. Technol.* **2021**, *278*, 119605.
[26] R. Baccar, M. Sarrà, J. Bouzid, M. Feki, P. Blánquez, *Chem. Eng. J.* **2012**, *211*, 310.
[27] N. K. Haro, P. Del Vecchio, N. R. Marcilio, L. A. Féris, *J. Cleaner Prod.* **2017**, *154*, 214.
[28] V. Arya, L. Philip, *Microporous Mesoporous Mater.* **2016**, *232*, 273.
[29] A. V. Dordio, S. Miranda, J. P. Prates Ramalho, A. J. P. Carvalho, *J. Hazard. Mater.* **2017**, *323*, 575.
[30] a) S. Shi, Y. Fan, Y. Huang, *Ind. Eng. Chem. Res.* **2013**, *52*, 2604; b) E.-S. I. El-Shafey, H. Al-Lawati, A. S. Al-Sumri, *J. Environ. Sci.* **2012**, *24*, 1579.
[31] L. Liu, X.-B. Luo, L. Ding, S.-L. Luo, in *Nanomaterials for the Removal of Pollutants and Resource Reutilization*, (Eds: X. Luo, F. Deng), Elsevier, Amsterdam **2019**, p. *83*
[32] S. Ain, R. Singh, Q. Ain, *Int. J. Pharm. Pharm. Sci.* **2016**, *8*, 160.
[33] a) D. Kong, D. Zhang, H. Guo, J. Zhao, Z. Wang, H. Hu, J. Xu, C. Fu, *Polymers* **2019**, *11*, 440; b) J. Wang, F. Ma, W. Liang, R. Wang, M. Sun, *Nanophotonics* **2017**, *6*, 943.
[34] I. Sengupta, S. Chakraborty, M. Talukdar, S. K. Pal, S. Chakraborty, *J. Mater. Res.* **2018**, *33*, 4113.
[35] B. Babu, S. Gupta, *i-Manager's J. Future Eng. Technol.* **2004**, *1*, 60.
[36] Y. Chen, X. Wang, C. Yu, J. Ding, C. Deng, H. Zhu, *Sci. Rep.* **2019**, *9*, 1.
[37] D. Swami, P. K. Sharma, C. S. P. Ojha, *Sadhana* **2014**, *39*, 1425.